

2D kinematic study of the central region of NGC 4501.

P. Repetto^{1*}, M. Faúndez-Abans¹, P. Freitas-Lemes^{2,4}, I. Rodrigues²,
M. de Oliveira-Abans^{1,3} †

¹*Laboratório Nacional de Astrofísica, Rua Estados Unidos 154, 37504-364, Itajubá, MG, Brazil*

²*Universidade do Vale do Paraíba, UNIVAP. Av. Shishima Hifumi, 2911, Urbanova CEP: 12244-000, São José dos Campos, SP, Brazil*

³*UNIFEI, Instituto de Engenharia de Produção e Gestão, Av. BPS 1303, Pinheirinho, 37 500-903, Itajubá, MG, Brazil*

⁴*Departamento de Física, Instituto Tecnológico de Aeronáutica (ITA), São José dos Campos, 12228-900, SP, Brazil*

Accepted xxxx XXXXXXXX 15. Received 2014 January 15; in original form 2014 January 15

ABSTRACT

GMOS-IFU observational data were used to study the detailed two dimensional gas kinematics and morphological structures within the $\sim 500 \times 421$ pc² of the active Seyfert 2 galaxy NGC 4501. We provide empirical evidences of possible outflowing material from the central zones of NGC 4501 to the observer. In addition, we performed a spectral synthesis and diagnostic diagram analysis to determine respectively the dominant stellar population in the inner disc of this galaxy and to unveil the actual nature of the central engine of NGC 4501. The principal finding of this work is that the central regions of NGC 4501 are dominated by non circular motions connected to probable outflows of matter from the nuclear regions of this galaxy. A predominant old stellar population inhabits the internal zones of NGC 4501 excluding the possibility of ongoing starburst activity in the central parsecs of this galaxy. The latter result is confirmed by the diagnostic diagram analysis that establishes a preponderant active galactic nucleus character for NGC 4501. These outcomes together provide a general description of the gas motion and the corresponding nuclear activity in the internal disc of NGC 4501 in an attempt to elucidate the possible relation among the central activity and the induced kinematic properties of this nearby galaxy.

Key words: galaxies: active. galaxies: individual: NGC 4501. galaxies: evolution. galaxies: Seyfert. galaxies: spiral

1 INTRODUCTION

Nearby galaxies with active galactic nucleus (AGN) are good laboratories to study and understand how mass is transferred from galactic scales down to nuclear scales to feed a supermassive black hole. Theoretical models and simulations have suggested that non-axisymmetric potentials promote gas inflow towards the inner regions of an AGN (Shlosman et al. 1990; Emsellem et al. 2003; Knapen 2005; Englmaier & Shlosman 2004). Observations of the inner kiloparsec of AGNs revealed the existence of some morphological structures such as inner small-scale disks, nuclear bars and spiral-like arms (Erwin & Sparke 1999; Pogge & Martini 2002; Laine et al. 2003). Martini et al. (2003) estimated that in more than half of AGNs the most common nuclear kiloparsec structures are dusty spirals. This supports the idea that those inner spiral-like arms could be part of the fuelling

chain to the central engine, by transporting gas from the outside kiloparsec down to a few tens of parsecs (Knapen et al. 2000; Emsellem et al. 2001; Maciejewski et al. 2002; Marconi et al. 2003; Crenshaw et al. 2003; Fathi et al. 2005, 2006; Maciejewski 2004). Fathi et al. (2005) and Storchi-Bergmann et al. (2007) mapped the streaming motion of gas towards the nuclei of the active galaxies NGC 1097 SB(s)b, and NGC 6951 SAB(rs)bc. Prieto et al. (2005) discovered spiral structure within the inner 300 pc of the LINER/Seyfert 1 galaxy NGC 1097. Using near-infrared high resolution images obtained with the ESO-VLT, they reported and argued that these spirals trace cool dust streams, and that they could be the channels by which cold gas and dust flow to a nuclear supermassive black hole. Recent works, mostly in the near-infrared, have analysed several nearby galaxies and revealed the presence of different nuclear morphological structures (disk-like, bar-like, spiral-like) responsible for transferring the material from kpc scales down to tens of pc scales (Riffel et al. 2008; Storchi-Bergmann et al. 2010; Riffel & Storchi-Bergmann 2011; Riffel et al. 2013; Schnorr-Müller et al. 2014).

* E-mail: prsatch6@gmail.com

† Based on observations obtained at the Gemini Observatory acquired through the Gemini Science Archive.

The Virgo spiral galaxy NGC 4501 (M88), a Seyfert 2 galaxy, is at a distance of 16.1 Mpc (Ferrarese et al. 1996). This galaxy, an SA(rs)b Hubble type (de Vaucouleurs et al. 1991), was studied by Silchenko et al. (1999) using the Multi-pupil Field Spectrograph attached to the 6-m telescope of the Special Astrophysical Observatory, who found a chemically decoupled nucleus within a radius less than 234 pc. Onodera et al. (2004), using the Nobeyama Millimeter Array, presented a CO (1-0) 2D kinematic analysis of the central 5 kpc region of NGC 4501. The main finding was a central gas concentration with a radius of 390 pc, formed by two double peaks separated by 370 pc. These authors interpreted this gas concentration as originating from gas transfer to the central region by a density wave perturbation due to the spiral arms. Mazzalay et al. (2014) accomplished a 2D gaseous and stellar kinematic study of the central 240×240 pc² of NGC 4501 with SINFONI/VLT in the H₂ 2.12 μ m line and detected a blueshifted chain of gas that was interpreted as an outflow in the North-West direction beginning near the centre of NGC 4501 up to 120 pc.

NGC 4501 is undergoing early stage ram pressure stripping, as suggested by some authors (Kenney et al. 2004; Crowl et al. 2005; Vollmer et al. 2007, 2008; Vollmer 2009; Vollmer et al. 2012), and shows three to four times less HI than expected for a “normal” galaxy. This galaxy seems to be in a pre-peak phase of ram pressure stripping (Vollmer et al. 2008). An X-ray luminosity of $L_X = 3.5 \times 10^{38}$ erg s⁻¹ (Li & Wang 2013) and a bolometric luminosity of $L_{Bol} = 4.17 \times 10^{39}$ erg s⁻¹ (Wu et al. 2013) are reported for NGC 4501 that is close enough to have its central hundreds of parsecs covered by an Integral Field Unit (IFU) instrument, in order to map and verify the existence of streaming motions in the nuclear area.

We present two-dimensional maps of the gas kinematics and structure within the inner $\sim 500 \times 421$ pc² of NGC 4501. This work is based on observational data acquired through the Gemini Science Archive, gathered with Gemini Multi Object Spectrograph and its Integral Field Unit (GMOS-IFU) (Allington-Smith et al. 2002).

2 OBSERVATIONS AND DATA REDUCTION

We used data from the Gemini Science Archive, obtained with the GMOS-IFU at Gemini North telescope, using the R400-G5305 grating and *r*-G0303 filter. The three IFU fields in the GMOS pointing image, the Lucy Richardson Deconvolution, and a Low-Pass filtered image are displayed in Figure 1. The position angle of the IFU fields is 140°, coincident with the photometric position angle of the major axis of NGC 4501. The central IFU field is centred at $\alpha = 12^h31^m59.22^s$ and $\delta = +14^\circ25'12.69''$ (J2000), corresponding to the photometric centre of this galaxy. The GMOS-IFU consists of 1000 science-object fibres (each one of diameter 0.2'') arranged in a rectangular array of size $7'' \times 5''$. The spectral setup gave a wavelength coverage of 5600–7000 Å at a spectral resolution of $R \approx 3500$ (85 km s⁻¹). Our IFU fields correspond to a rectangular array of $\sim 7'' \times 15''$. The spatial resolution of the data is $0.77''$ (~ 60 pc).

The standard Gemini-IRAF routines were used to carry out bias subtraction, flat-fielding, sky subtraction, and cos-

mic ray correction. The spectra were wavelength calibrated with an accuracy of ≤ 0.3 Å and flux-calibrated using the spectroscopic standard star Feige 66, a tertiary standard from Baldwin & Stone (1984), as revised by Hamuy et al. (1992). Finally, the produced data cubes were combined into one reduced cube with dimensions of 101×213 px² (about $\sim 7.34'' \times 15.5''$ and $\sim 572 \times 1209$ pc²). The field of view (FOV) of the analysed data were restricted in order to have data with a signal to noise ratio (S/N) of about 3–7 for the emission lines with the strongest signal (i.e. [N II]λ6584 and Hα), in the range of 88×74 px² (about $\sim 6.4'' \times 5.4''$ and $\sim 500 \times 421$ pc²). In the case of the NaIDλ5892 absorption line, we fixed the boundaries of our analysed FOV to the interval $\sim 41 \times 47$ px² (about $\sim 3.0'' \times 3.4''$ and $\sim 234 \times 265$ pc²), to obtain S/N in the same range.

Figure 2 shows one integrated spectrum in the central $\sim 0.6 \times 1.2$ kpc² of NGC 4501. It reveals the presence of [O I]λ6300, Hα, [N II]λλ6548, 6584, [S II]λλ6717, 6731 emission lines and the NaIDλ5892 absorption line.

3 RESULTS

3.1 Kinematic analysis: synopsis and methodology

We constructed the continuum flux, monochromatic flux, velocity field, Full Width at Half Maximum (FWHM), and equivalent width maps for all the lines of the individual spectra, with the exception of [O I]λ6300 whose S/N ratio is less than 2. The centroid velocities, the fluxes, FWHM and the equivalent width of the observed lines were obtained by fitting single Lorentzian profiles to each single line, through the IRAF¹ task *fitprofs*. Tailored PyRAF-based scripts were used to perform the fitting task and to produce the 2D maps for each line. The Lorentzian profiles fitted the actual line peaks and wings better than the Gaussian profiles, consequently we adopted Lorentzian profiles to derive from the data radial velocities, FWHMs, equivalent widths and fluxes.

We obtained full spatial maps only for [N II]λ6584 and Hα, due to the more extended and stronger emission with respect to all the remaining lines. In the case of NaIDλ5892, we constructed smaller maps for the spatial points with the strongest absorption. The maps of [N II]λ6548 and [S II]λλ6717, 6731, contain very few points with strong emission, and the kinematics is complex enough to prevent a straightforward interpretation; therefore we do not show any maps for these three lines. The line fluxes, FWHM, and equivalent width maps of [N II]λ6584 and Hα are shown in Figures 3 and 4.

We corrected the FWHM maps for instrumental resolution, whose value corresponds to $\sim 0.31''$ (~ 4.26 pxls). The errors were estimated by means of Monte Carlo simulations using Poisson statistic model for the data (as already implemented in the *fitprofs* task). The result was that the measurement errors are less than 5% in the case of the continuum and line flux and less than 5 km s⁻¹ for FWHM,

¹ IRAF is distributed by the National Optical Astronomy Observatory, which is operated by the Association of Universities for Research in Astronomy (AURA) under cooperative agreement with the National Science Foundation.

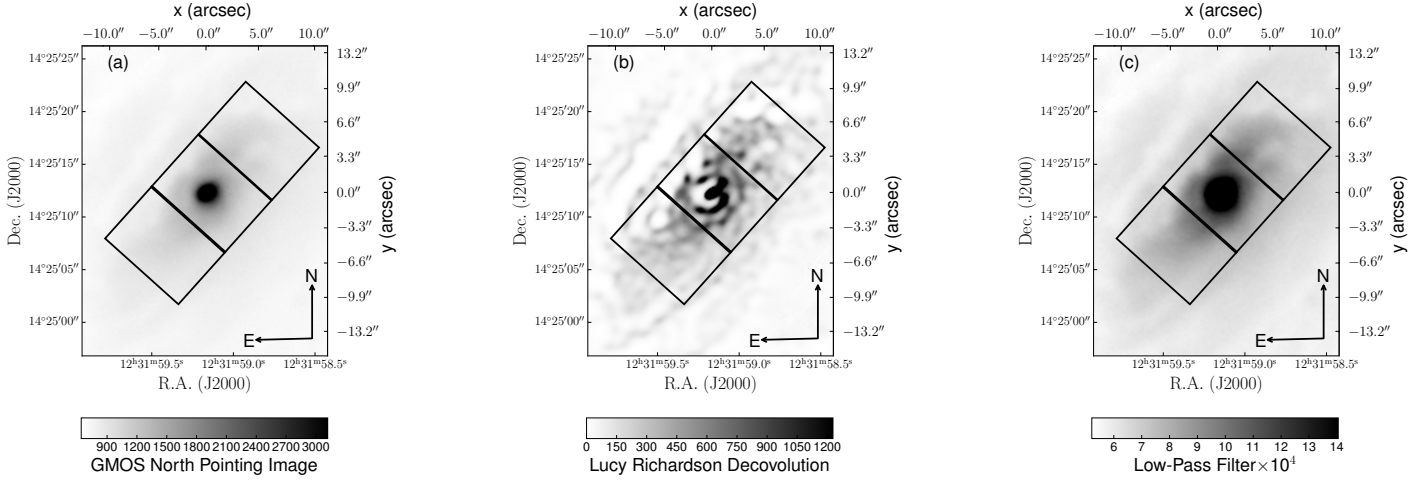


Figure 1. (a): Original optical 10-min exposure GMOS-N image in the r-G0303 filter, P.A.=140°. (b): Lucy-Richardson deconvolution applied to the same image. (c): Low-Pass filtered image. The three IFU fields are outlined by black boxes. The colorbar units are counts.

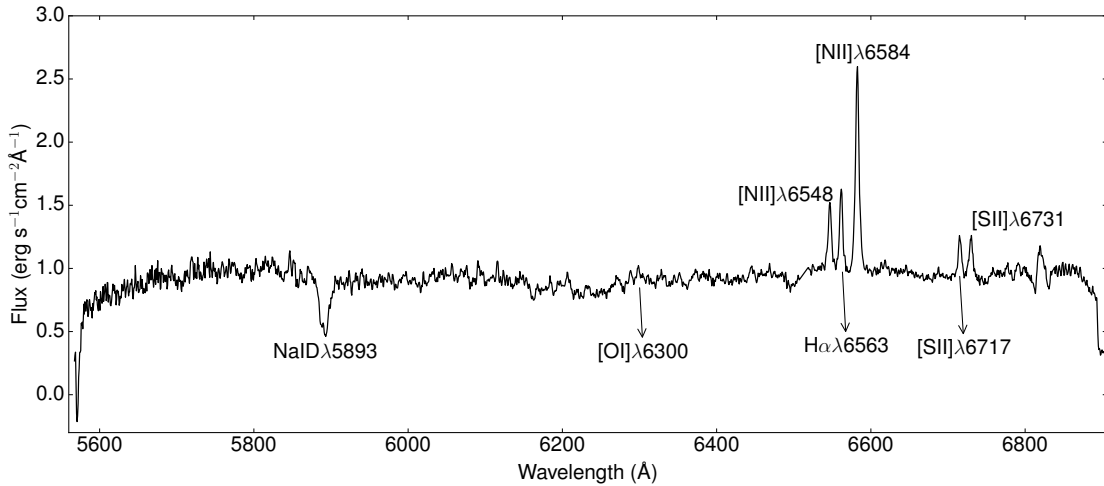


Figure 2. The nuclear spectrum of NGC4501, displayed in units of $10^{-16} \text{ erg sec}^{-1} \text{ cm}^{-2} \text{ Å}^{-1}$, with the emission and absorption lines marked. The kinematic maps were derived for the strongest emission lines [N II] $\lambda 6584$, $\text{H}\alpha$, and also for the absorption Sodium line.

equivalent width and radial velocity. We do not show the continuum fluxes, given that the information presented in these maps are very similar to that displayed in the first panels of Figures 3 and 4. Following, we detail the analysis of the 2D observed velocity fields of [N II] $\lambda 6584$ and $\text{H}\alpha$.

3.1.1 Kinematics of [N II] $\lambda 6584$ and $\text{H}\alpha$

In an attempt to model the observed velocity fields (OVFs) of [N II] $\lambda 6584$ and $\text{H}\alpha$ we applied the 2D Locally Weighted Multivariate Regression (LOESS) algorithm of Cleveland & Devlin (1988) through the python implementation of Cappellari et al. (2013) to remove noisy regions that could affect the determination of the kinematic position angle (KPA). The KPA of the OVFs of [N II] $\lambda 6584$ and $\text{H}\alpha$ is 114° , however the KPA of the filtered LOESS velocity fields (LVFs)

of both lines is 137° . The LVFs exhibit relevant non-circular motions, which is the main motivation to produce synthetic velocity fields (SVFs) for [N II] $\lambda 6584$ and $\text{H}\alpha$ to recover gas rotation and expansion velocities. This sort of 2D phenomenological modelling should give us more insights on the azimuthal, radial and vertical gravitational forces that rule the gas kinematic in the inner zones of NGC 4501. The analysis of the LVFs was performed considering the relation first reported by Rogstad (1971):

$$V_{\text{obs}}(x, y) = V_{\text{sys}} + [V_{\text{Rot}}(R) \cos \theta + V_{\text{exp}}(R) \sin \theta] \sin i \quad (1)$$

where V_{obs} is the observed radial velocity at sky coordinates x and y , V_{sys} is the systemic velocity, V_{Rot} is the rotation velocity, V_{exp} is the expansion velocity, R is the radius in the plane of the galaxy, i is the inclination (INCL) of the plane of the galaxy with respect to the line of sight and θ

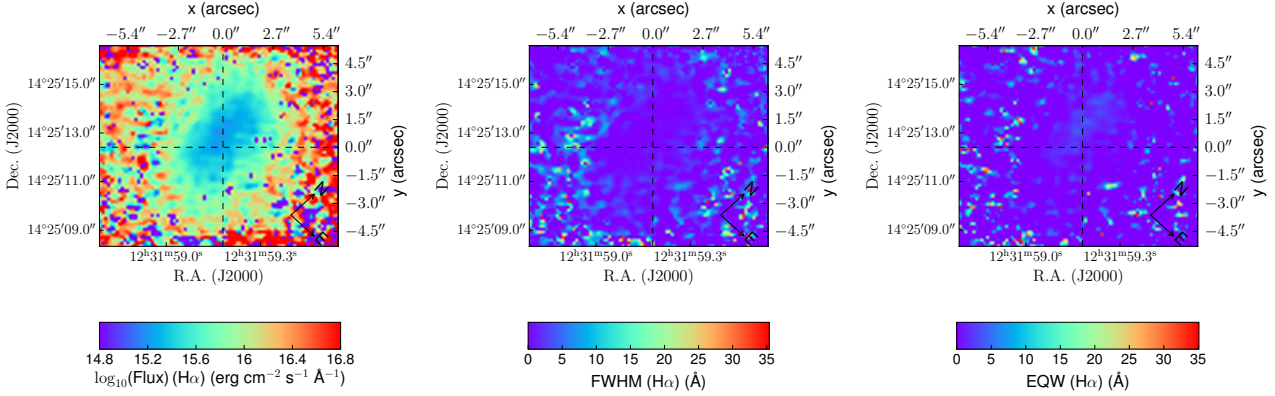


Figure 3. Left panel: logarithm of the observed monochromatic flux of [N II]λ6584. Middle panel: Lorentzian FWHM of [N II]λ6584. Right panel: equivalent width of [N II]λ6584.

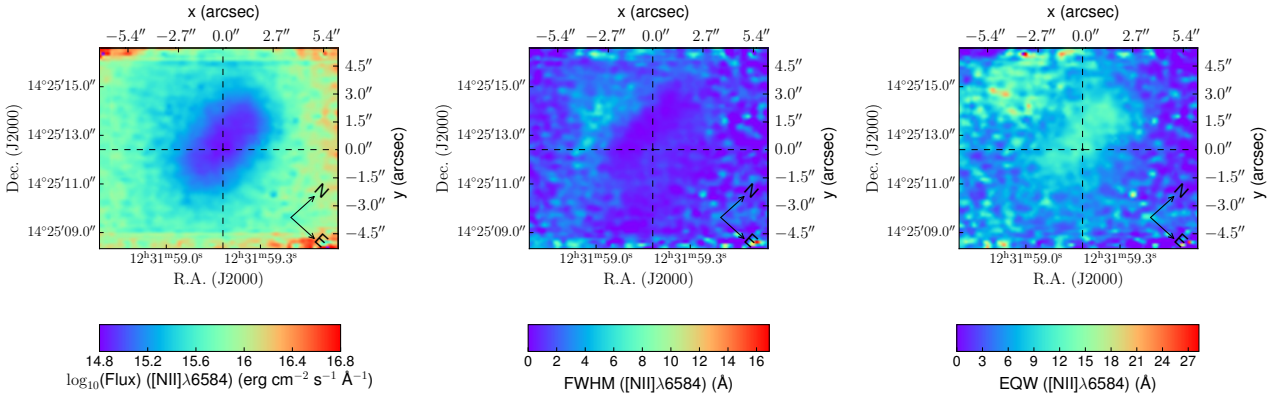


Figure 4. Left panel: logarithm of the observed monochromatic flux of Hα. Middle panel: Lorentzian FWHM of Hα. Right panel: equivalent width of Hα.

is the azimuthal angle in the plane of the galaxy given as a function of INCL and KPA.

We assumed an exponential disk (Freeman 1970) as a first guess for the rotation velocity and we deduced an expansion velocity by a trial-and-error iterative fitting method aimed to minimize the residual velocity fields (RVFs), obtained subtracting the SVFs to the LVFs. In the fitting process the galaxy photometric centre ($\alpha = 12^{\text{h}}31^{\text{m}}59.22^{\text{s}}$ and $\delta = +14^{\circ}25'12.69''$ (J2000)) and the systemic velocity ($V_{\text{sys}} = 2214 \text{ km s}^{-1}$) were fixed. The expansion velocity that returned the minimum RVFs was $V_{\text{exp}}(R) = R^{\alpha} + \ln(R)$ with $\alpha = 0.75 \pm 0.005$ and a maximum value of $\sim 25 \text{ km s}^{-1}$. We also examined Plummer (Plummer 1911), Hernquist (Hernquist 1990) and Logarithmic (Binney & Spergel 1984) rotation velocities, yet the least RVFs were obtained with the exponential disk model with a maximum value of $\sim 3 \text{ km s}^{-1}$. The general conclusion of the kinematic analysis of [N II]λ6584 and Hα was that the LVFs were better reproduced by the exponential disk model and the expansion velocity given above; the best fitted kinematic parameters are $KPA = 137^{\circ} \pm 3^{\circ}$ and

$INCL = 61^{\circ} \pm 2^{\circ}$, in accordance with the corresponding photometric parameters. The LVFs and the SVFs are dominated by the expansion velocity component as one can realize from the reported maximum of both velocity components. The OVFs, LVFs, SVFs and RVFs are displayed in Figures 5 and 6.

3.2 Outflow detection in the inner disc of NGC 4501

The NaIDλ5892 absorption line has a low ionization potential (5.1 eV), therefore it is expected to originate in those regions of the interstellar medium shielded from ultraviolet radiation, where the hydrogen is mostly neutral. It has been used, by some authors, as a tracer of inflow and outflow of the neutral atomic gas phase in the interstellar medium (Phillips 1993; Heckman et al. 2000; Rupke et al. 2005; Davis et al. 2012; Rupke & Veilleux 2015).

The NaIDλ5892 velocity field of NGC 4501 shows filamentary structures that could represent possible gas fuelling

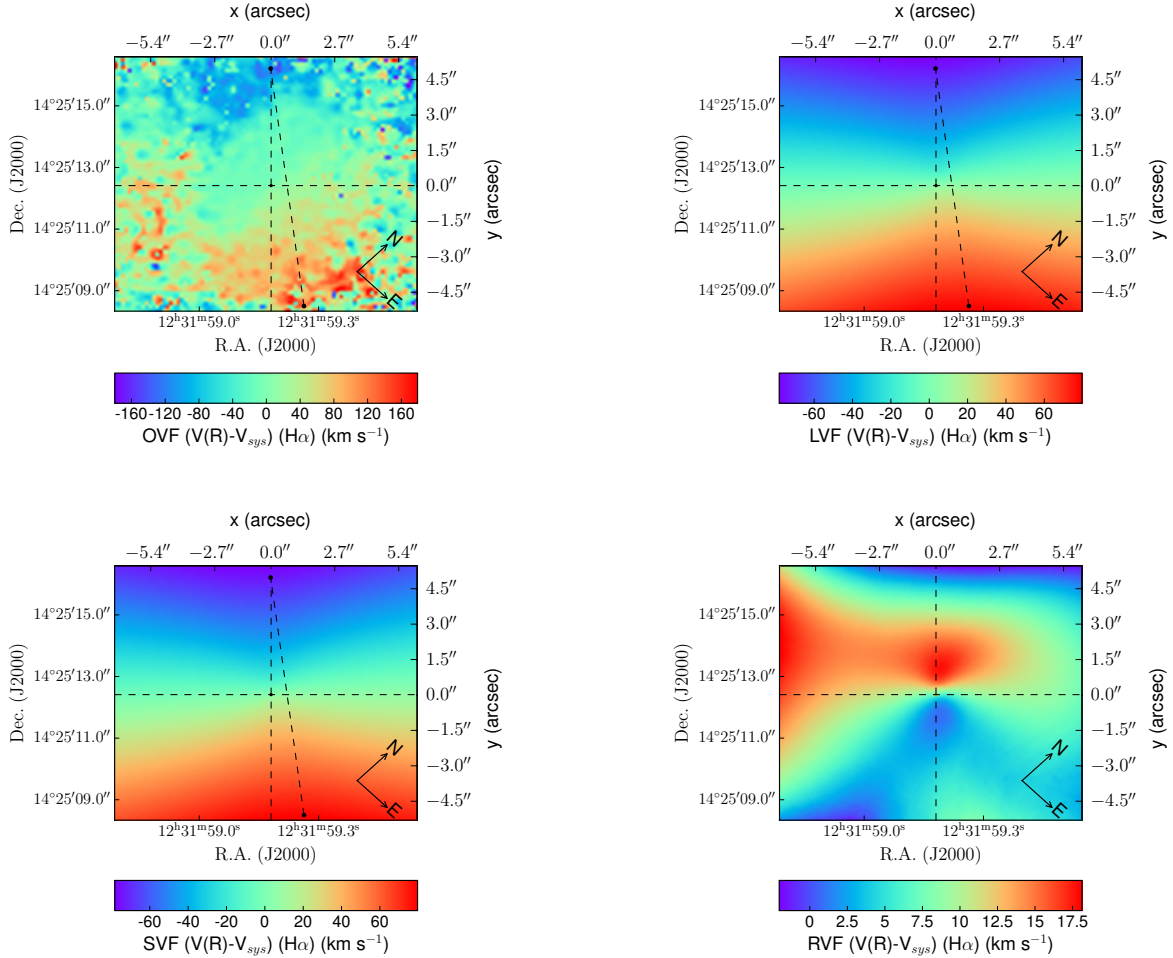


Figure 5. Top left: observed velocity field of $[\text{N II}]\lambda 6584$. Top right: LOESS filtered velocity field of $[\text{N II}]\lambda 6584$. Bottom left: synthetic velocity field of $[\text{N II}]\lambda 6584$. Bottom right: residual velocity field of $[\text{N II}]\lambda 6584$. The dashed line connects the two points with maximum velocity gradients denoting the kinematic position angle of NGC 4501.

towards or from the central regions of this galaxy as denoted by the green dashed lines (numbers 1 and 2) in Figure 7.

Basically, to probe the gas inflow or outflow in a galaxy disc, we need some criteria to establish the actual orientation of this particular galaxy in the sky. The same information is needed to decide whether a given galaxy has trailing or leading spiral arms. Sharp & Keel (1985) (SK85 hereafter), following de Vaucouleurs (1958) and Holmberg (1947), give a robust general recipe to ascertain whether a particular spiral galaxy has leading or trailing arms. Their prescription is based on three main pieces of information: (1) receding-approaching side, (2) direction of rotation of spiral arms and (3) the tilt of the galaxy (i. e. nearer and farther side to the observer). The same authors showed that the interacting spiral galaxy NGC 5395 has trailing arms, contrary to the claim by Pasha & Smirnov (1982) of a possible candidate with leading arms. Väisänen et al. (2008) used the SK85 method to determine that the luminous infrared galaxy IRAS 18293-3413 has a pair of leading arms. Repetto et al. (2010) employed the same methodology to show that

the interacting galaxy pair KPG 390 is a trailing pair of spirals.

The two first criteria of SK85 are obvious for NGC 4501, from the 2D kinematic information collected in this work and from the kinematic of the entire disc of NGC 4501 (Chemin et al. 2006) (1) and also, for instance, from the SDSS photometry in the g band available in the literature for this galaxy (Adelman-McCarthy et al. 2006) (2). The third criterion of SK85, the tilt of NGC 4501, could be determined if there were dust lanes around the galactic nucleus and, if this were the case, the nearest side would be the one which presents the higher difference in intensity than the farthest side, as discussed by SK85.

Carollo et al. (1998) (CA98 hereafter) analysed Wide Field Planetary Camera 2 (WFPC2) F606W image data of 40 spiral galaxies, including NGC 4501, providing morphological and photometric properties for the entire sample. These authors displayed the $18'' \times 18''$ of the nuclear region of NGC 4501 unveiling spiral-like dust lanes surrounding the nucleus.

In Figure 8 we show an intensity profile extracted from

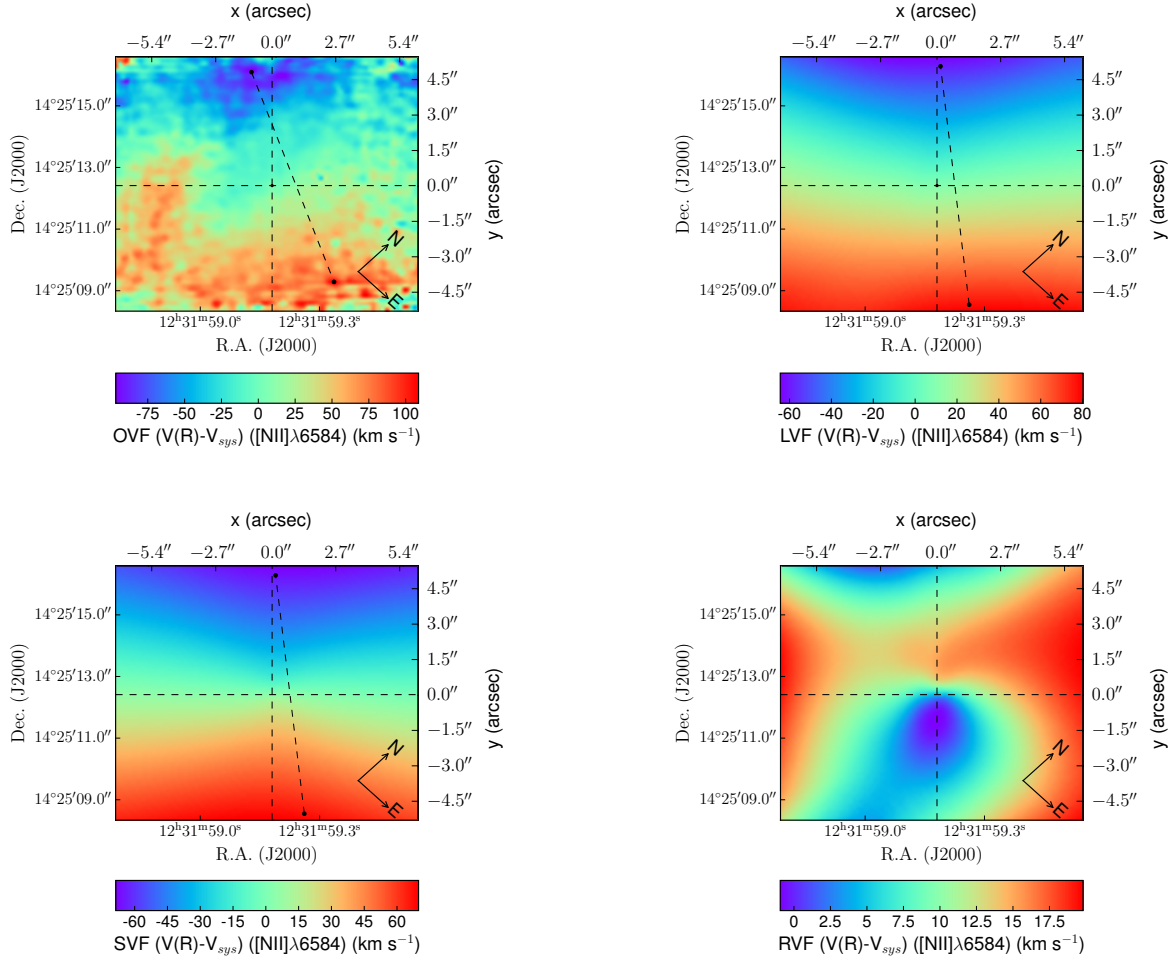


Figure 6. Top left: observed velocity field of $H\alpha$. Top right: LOESS filtered velocity field of $H\alpha$. Bottom left: synthetic velocity field of $H\alpha$. Bottom right: residual velocity field of $H\alpha$. The dashed line connects the two points with maximum velocity gradients denoting the kinematic position angle of NGC 4501.

the WFPC2 F606W image studied by CA98, to determine which side of NGC 4501 is nearer to the observer.

The application of the strategy of SK85 to NGC 4501 produced the following results:

1) The approaching radial velocities are in the north-western (NW) side of NGC 4501, whereas the receding radial velocities are in the southeastern (SE) part as suggested by Figures 5 and 6, therefore the direction of rotation of the disc of NGC 4501 is clockwise.

2) The tips of the spiral arms of NGC 4501 point in a counter-clockwise direction as readily noticed from the SDSS g band image showed in Figure 8.

3) It is evident from Figure 8 that the nearest part of NGC 4501 to the observer is the NE side, because the profile descends more abruptly than along the SW side.

From these three evidences and Figure 8 we concluded that the filamentary structures S1-S5 and S6-S10 observed in the NaID λ 5892 velocity field of Figure 7 correspond to outflowing gas towards the observer and that NGC 4501 has trailing arms.

Other empirical proofs of streaming material from the

nuclear regions of NGC 4501 to the observer arise from the analysis of the velocity profiles of the two spiral-like structures S1-S5 and S6-S10 presented in Figure 9. The radial velocity of these two pseudo-arms with respect to the central systemic velocity are in the range $10 \text{ km s}^{-1} < \Delta V < 80 \text{ km s}^{-1}$ showing complex gas and dust motion along these inner spirals. The kinematics of [NII] λ 6584 and $H\alpha$ suggests that the gas in the central $500 \times 421 \text{ pc}^2$ of NGC 4501 is receding to the observer in the S-E and E and approaching to us in the N-W and W. The NaID λ 5892 velocity field largely follow the gas kinematics showing clumps and segmented arm-like structures approaching us.

On the other side, Mazzalay et al. (2014) found evidences of outflow from the central regions of NGC 4501. In spite of the different spatial resolution of their data ($< 15 \text{ pc}$) and the distinct tracer they used ($\text{H}_2 \text{ } 2.12 \text{ } \mu\text{m}$), the black crosses in Figure 7 show a tentative location of their outflow detection.

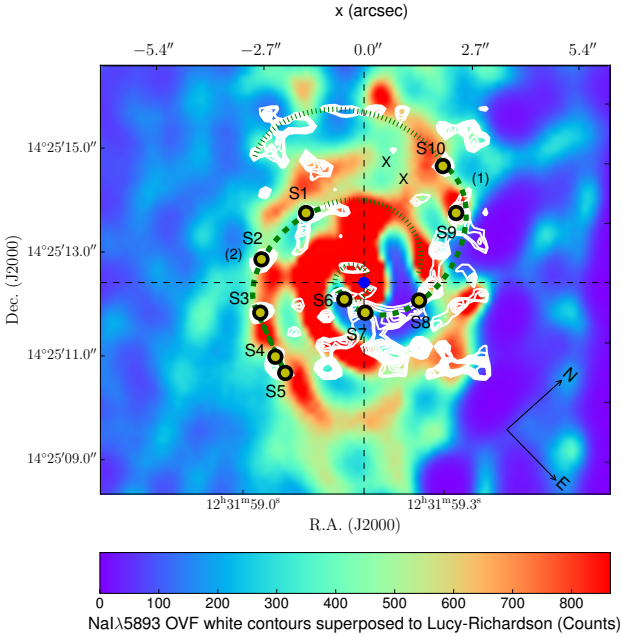


Figure 7. Clipped Lucy-Richardson Deconvolution image with superposed white contours of the region of NaIDλ5892 OVF which indicates the presence of a possible outflow. The green dashed lines suggest possible outflow paths from the central regions of NGC 4501. The white contour levels of the NaIDλ5892 OVF correspond to the radial velocities range from 30 to 102 km s⁻¹ separated by a step of 8 km s⁻¹. The blue dot is the kinematical centre.

4 SPECTRAL SYNTHESIS

The detailed study of the star formation provides important information on the age distribution along their stellar population components (Krabbe et al. 2011); (Faúndez-Abans et al. 2015); (Dors et al. 2016). We investigate the star formation history of NGC 4501 using the stellar population synthesis code STARLIGHT (Cid Fernandes et al. 2004, 2005); (Mateus et al. 2006); (Asari et al. 2007).

This code is extensively discussed in Cid Fernandes et al. (2004, 2005), and is built upon computational techniques originally developed for empirical population synthesis with additional ingredients from evolutionary synthesis models. Briefly, the code fits an observed spectrum with a combination of N_* single stellar populations (SSPs) from the Bruzual & Charlot (Bruzual & Charlot 2003) (BC03) models. These models are based on a high-resolution library of observed stellar spectra, which allows for detailed spectral evolution of the SSPs across the wavelength range of 3200-9500 Å with a wide range of metallicities. We used the Padova's 1994 tracks, as recommended by BC03, with the initial mass function of Chabrier (2003) between 0.1 and 100 M_{\odot} . Extinction is modeled by STARLIGHT as due to foreground dust, using the Large Magellanic Cloud average reddening law of Gordon et al. (2003) with $R_V = 3.1$, and parametrized by the V-band extinction A_V . The SSPs used in this work cover 15 ages, $t = 0.001, 0.003, 0.005, 0.01, 0.025, 0.04, 0.1, 0.3, 0.6, 0.9, 1.4, 2.5, 5, 11, \text{ and } 13$ Gyr,

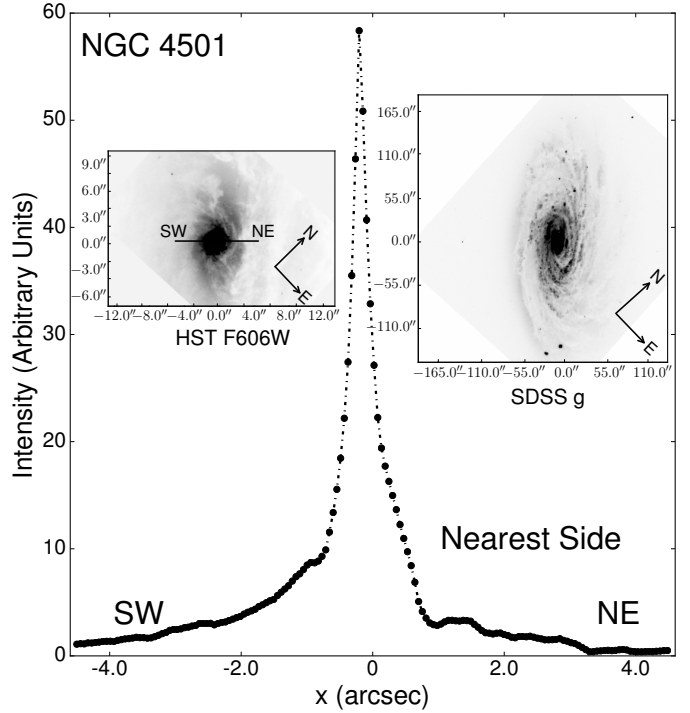


Figure 8. Intensity profile along the kinematic minor axis of NGC 4501. Left: HST F606W image of NGC 4501 from which the intensity profile was derived, the NE side is the nearest to the observer because the profile is more abrupt than along the SW part. Right: SDSS g band image of NGC 4501 illustrating the counter-clockwise direction pointed by the spiral arms tips of this galaxy.

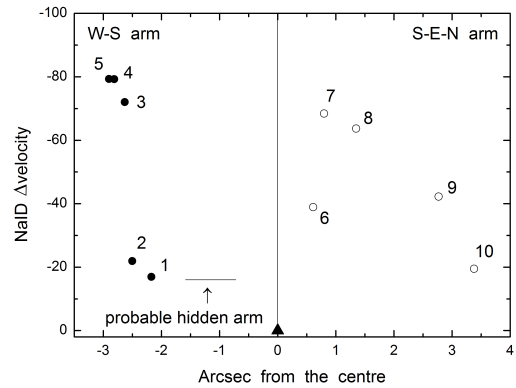


Figure 9. The probable outflow arms tracer divided arbitrarily in W-S and S-E-N regions. The NaIDλ5892 velocity difference from the central systemic one are displayed. The two likely chains of outflow S1-S5 and S6-S10 regions of Figure 7 are showed (filled and open circles respectively), and a plausible hidden arm section are highlighted. The filled triangle represents the kinematical centre. The N-E direction is the same of Figure 7.

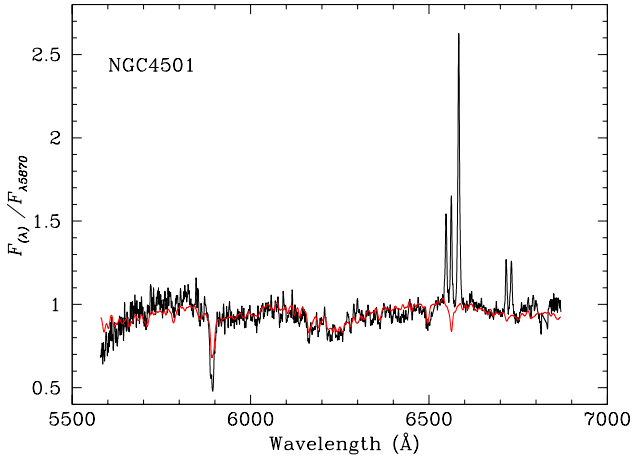


Figure 10. Stellar population synthesis for the nuclear region of NGC 4501. The figure shows the central bin observed spectrum corrected for reddening (black) and the synthesized spectrum (red).

and three metallicities, $Z = 0.2 Z_{\odot}$, $1 Z_{\odot}$, and $2.5 Z_{\odot}$, adding to 45 SSP components. The fitting is carried out using a simulated annealing plus Metropolis scheme, with regions around emission lines and bad pixels excluded from the analysis.

Figure 10 shows of the observed spectrum corrected by reddening and the model stellar population spectrum for the nuclear region of NGC 4501. Following the prescription of Cid Fernandes et al. (2005), we defined a condensed population vector, by binning the stellar populations according to the flux contributions into young, x_Y ($t \leq 5 \times 10^7$ yr); intermediate-age, x_I ($5 \times 10^7 < t \leq 2 \times 10^9$ yr); and old, x_O ($2 \times 10^9 < t \leq 13 \times 10^9$ yr) components. The results indicate that the central region is dominated by an old stellar population with age of $2 \times 10^9 < t \leq 13 \times 10^9$ yr. However, a small but non-negligible fraction of young (about 20 %) and intermediate (about %10) stars are also present. The quality of the fitting result is measured by the parameters χ^2 and $adev$, whose values are 1.1 and 4.35, respectively. The latter gives the perceptual mean deviation $|O_{\lambda} - M_{\lambda}|/O_{\lambda}$ over all fitted pixels, where O_{λ} and M_{λ} are the observed and model spectra, respectively. We found $A_V = 0.48$ mag and $Z = 1 Z_{\odot}$.

5 DIAGNOSTIC DIAGRAM OF THE CENTRAL REGIONS OF NGC 4501

To confirm the main ionizing mechanism of the central 500×421 pc² of NGC 4501, we used the diagnostic diagram introduced by Lamareille et al. (2009) (LM09).

This diagram is an instrument for a preliminary classification of galaxies, based on their $\log[S II](\lambda 6717 + \lambda 6731)/H\alpha$ and $\log[N II]\lambda 6584/H\alpha$ abundances, that separates objects ionized only by massive stars from those containing active nuclei. The diagram for the inner parsecs of NGC 4501 is displayed in Figure 11, where the SW, NE, and central zones of NGC 4501 are defined as in Figure 7.

Freitas-Lemes et al. (2012), in a study of the Polar Ring

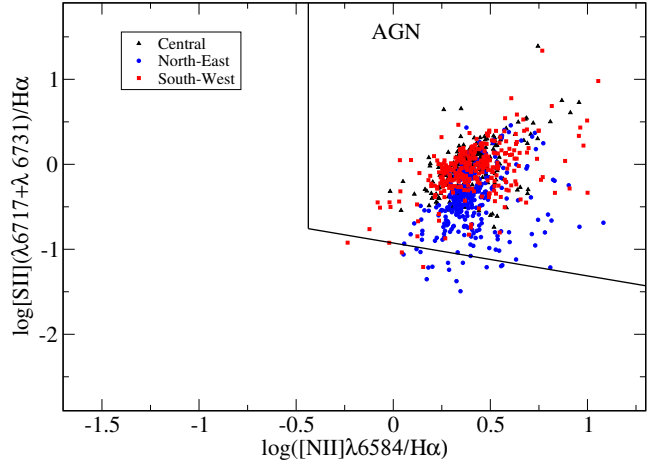


Figure 11. Diagnostic diagram $\log[S II](\lambda 6717 + \lambda 6731)/H\alpha$ versus $\log[N II]\lambda 6584/H\alpha$ for the nuclear region of NGC 4501. The lines correspond to the separation between narrow-line AGNs and H II galaxies as proposed by LM09. Black triangles represent measurements at the very centre region, blue circles, NE, and red squares, SW regions. The north-east direction is the same of Figure 7

galaxy AM 2020-504 and two interacting HII galaxies of the system AM 2229-735, and Faúndez-Abans et al. (2009) in the analysis of the peculiar ring galaxy HRG 54103, using the LM09 tool, found that the measurements of several regions on the rings were continuously distributed over an area which extended upwards from the HII part of the diagram to the AGN one, towards the locus of the AGN nucleus' measurement.

The AGN character of NGC 4501 is well established. This diagram suggests the existence of some stratification between the central, SW, and NE regions of the central structures of this galaxy. In Figure 11, the top triangles and blue circles are from the nuclear signal approaching us, the rest of the blue circles are from the NE region, and the red squares are measurements in the SW region receding from the observer.

6 DISCUSSION

The study of the nuclear morphological structures formed through the transport of material towards the central regions of galaxies represents a fundamental topic to understand the complex phenomenon of nuclear activity. As mentioned in the Introduction, several central structures have been already identified and analysed from a kinematic and physical point of view, in some galaxies, establishing a scenario where nuclear bar-like, disk-like, and spiral-like features are playing a pivotal role in the transfer of gas up to scales of tens-of-parsecs. At the present time, the number of studied galaxies is small, and it is difficult to overcome the tens of parsecs limit. Nevertheless, the above-mentioned studies represent a first and fundamental step to achieve a deeper understanding of the physics and kinematics that rule the fuelling of the central engine.

Bearing in mind the framework settled by these previous works and with similar spatial resolution, the present

analysis attempts to find evidence of kinematic structures that could be connected with the streaming motion of gas towards the centre of NGC 4501. We have used GMOS-IFU archival data to perform a detailed study of the 2D gas flux, radial velocity, FWHM, equivalent width and structures within the central $\sim 500 \times 421 \text{ pc}^2$ of the Seyfert 2 galaxy NGC 4501 a member of the Virgo cluster of galaxies. We used imaging filtering techniques and 2D kinematic analysis applied respectively to the GMOS pointing image and IFU data cube to investigate the streaming gas motion in the inner zones of NGC 4501.

Additionally we provide evidences of the prevailing AGN behaviour of NGC 4501 and the dominant old stellar populations residing in the interior disc of this galaxy separately through diagnostic diagram techniques and spectral synthesis analysis. The result of the spectral synthesis study confirms in part the AGN preponderance with respect to starburst in the inner hundreds of parsecs of NGC 4501.

The 2D kinematic of [N II] $\lambda 6584$ and H α gives some information about the amplitude of the stellar gravitational potential and the decoupling between stars rotation and gas diffusive motion in the inward regions of NGC 4501. A fundamental result of the 2D kinematic analysis is that gas diffusion dominates over stellar rotation in the central zones of NGC 4501 because of the decrease of the total stellar mass at smaller radii.

The plausible detection of outflowing material across the inner spiral arms S1-S5 and S6-S10, confirms the predominance of non circular motions and intricate gas and dust dynamics on different levels in the inner zones of NGC 4501.

In general galaxies are 3D aggregates of several gravitating constituents, principally stars, gas and dark matter. In the central regions of galaxies the gravitational contribution of dark matter can be neglected with respect to that of baryons according, for instance, to the analysis of [Linden \(2014\)](#). The author compares the masses of baryons and dark matter in the inner 100 pc of the Galaxy using the model of [McMillan \(2011\)](#) showing the gravitational predominance of baryons over dark matter, based on these results we decided to consider exclusively the stellar and gas gravitational components.

From a kinematic point of view, the 2D deprojection of the observed radial velocities of each point of an actual 3D galaxy originates a measure of the kinematic of all the gravitational components present in the analysed galaxy. The rotation and expansion velocity components extracted from a 2D velocity field generated by a 3D observed data cube of a given galaxy are valuable information about the dominant motions within this particular galaxy disc and allow, in principle, the separation of the kinematics of the stellar and gas components assuming prevalent circular movements associated to the stellar gravitational potential. These considerations are applicable to a real galaxy as far as the circular motions of the stars predominate over the radial and vertical streaming motions. The latter approximation could not completely hold in the central region of galaxies due to the increase of stellar random motions and the corresponding decrease of stellar ordered rotation.

In the Galaxy, some studies (see [Genzel et al. \(2010\)](#) for a complete set of references) depicted the composite stellar kinematics of the central regions with much more detail and

accuracy than for external galaxies, therefore, we shortly recapitulate those findings about the stellar motions in the inner zones of our galaxy in order to comment briefly about the results of the 2D gas kinematic analysis of NGC 4501.

The very central regions of our galaxy ($< 10 \text{ pc}$), as determined by stellar proper motion measurements, are mostly characterised by an overall rotation of old and young stars in a nuclear cluster and in a disc with different inclinations and position angles with respect to the sky plane respectively. Another component of massive O and Wolf-Rayet stars display azimuthal motion in the opposite direction to the disc of young stars mentioned above ([Trippe et al. 2008](#); [Schödel et al. 2009](#); [Paumard et al. 2006](#); [Lu et al. 2009](#)).

The actual stellar kinematical picture of the Galaxy could be much more complex and additional non circular motions could originate in the intersection between azimuthal motions on surfaces with different orientation with respect to the sky plane as indicated by the researches quoted above and also by other observational and theoretical studies ([Bartko et al. 2009](#); [Kocsis & Tremaine 2011](#)).

The kinematic analysis performed in the present work utilizes two emission lines ([N II] $\lambda 6584$ and H α) as gaseous tracers of the stellar gravitational potential of NGC 4501. Albeit we are aware that our knowledge of the stellar motion is indirect, the gaseous tracers could be influenced by physical forces other than gravity (e.g. radiative and magnetic force) and the spatial resolution of our data is good ($\sim 60 \text{ pc}$), but not so high as that of the quoted investigations about the Galaxy, in the particular case of NGC 4501 we successfully separate rotation from non circular motions and in conformity with previous works quoted in the Introduction we argue that, to a first approximation, the circular velocities detected in the inward zones of NGC 4501 primarily represent the remnant of the radial variation of the stellar gravitational potential, whereas the non circular velocities are more likely associated to gas radial and vertical (deprojected) motions. These findings, together with the other results derived in the present study of NGC 4501 constitute a suitable approach to disentangle the kinematic and physical conditions in the central disc of this galaxy. In particular, a future 3D kinematic analysis of NGC 4501 should take into account in a more realistic way the actual three dimensional kinematics of stars and gas and their interaction on different vertical levels of the disc of NGC 4501.

7 CONCLUSIONS

In this article we performed a 2D kinematic study of the inner regions of NGC 4501 in an attempt to ascertain the azimuthal and radial gas velocities in the internal disc of NGC 4501. We accomplished a spectral synthesis and diagnostic diagram analysis in an effort to deduce the true nature of the central engine of NGC 4501. We collected empirical evidences of outflowing material from the central parsecs of NGC 4501.

In summary our findings about the kinematical and physical properties of the inner $500 \times 421 \text{ pc}^2$ of NGC 4501 are the following:

- The central regions of NGC 4501 are dominated by expansion velocity probably associated to dissipative gas processes.

- Old stars predominate in the central zones of NGC 4501 suggesting weak or absent star formation activity.
- The central part of NGC 4501 exhibits a predominant AGN character.
- We detected two inner pseudo-spirals that likely represent chains of outflowing material from the centre of NGC 4501.

This work presents a combination of different analysis techniques to gather a broader knowledge about the kinematical and physical properties of the inner regions of NGC 4501. The itemized results elucidate some global aspects of the phenomenological behaviour of gas and stars in the central parsecs of NGC 4501.

ACKNOWLEDGMENTS

R. P. thanks LNA for postdoctoral fellowship through CNPq grant 313998/2013-2.

I. R. thanks the support of FAPESP agency, process 2013/17247-9.

P.F-L thanks the support of CAPES.

This work was partially supported by the Brazilian Ministério da Ciência, Tecnologia e Inovação (MCTI), Laboratório Nacional de Astrofísica (MCTI/LNA). Based on observations obtained at the Gemini Observatory (acquired through the Gemini Science Archive and processed using the Gemini IRAF package), which is operated by the Association of Universities for Research in Astronomy, Inc., under a cooperative agreement with the NSF on behalf of the Gemini partnership: the National Science Foundation (United States), the National Research Council (Canada), CONICYT (Chile), Ministerio de Ciencia, Tecnología e Innovación Productiva (Argentina), and Ministério da Ciência, Tecnologia e Inovação (Brazil). This research made use of the NASA/IPAC Extragalactic Database (NED), which is operated by the Jet Propulsion Laboratory, California Institute of Technology, under contract with the National Aeronautics and Space Administration. This research has made use of the NASA/IPAC Infrared Science Archive, which is operated by the Jet Propulsion Laboratory, California Institute of Technology, under contract with the National Aeronautics and Space Administration. Based on observations made with the NASA/ESA Hubble Space Telescope, and obtained from the Hubble Legacy Archive, which is a collaboration between the Space Telescope Science Institute (STScI/NASA), the Space Telescope European Coordinating Facility (ST-ECF/ESA) and the Canadian Astronomy Data Centre (CADC/NRC/CSA). We acknowledge the use of the Kapteyn package (Terlouw & Vogelaar 2012) and the ROOT package (Brun & Rademakers 1997). We used the CAPLOESS2D routine of Cappellari et al. (2013), which implements the 2D multivariate LOESS algorithm of Cleveland & Devlin (1988).

REFERENCES

Adelman-McCarthy J. K., Agüeros M. A., Allam S. S., 2006, *ApJS*, **162**, 38
Allington-Smith J., et al., 2002, *PASP*, **114**, 892

Asari N. V., Cid Fernandes R., Stasińska G., Torres-Papaqui J. P., 2007, *MNRAS*, **381**, 263
Baldwin J. A., Stone R. P. S., 1984, *MNRAS*, **206**, 241
Bartko H., Martins F., Fritz T. K., Genzel R., 2009, *ApJ*, **697**, 1741
Binney J., Spergel D., 1984, *MNRAS*, **206**, 159
Brun R., Rademakers F., 1997. AIHENP'96 Workshop, Lausanne, pp 81–86
Bruzual G., Charlot S., 2003, *MNRAS*, **344**, 1000
Cappellari M., McDermid R. M., Alatalo K., Blitz L., 2013, *MNRAS*, **432**, 1862
Carollo C. M., Stiavelli M., Mack J., 1998, *AJ*, **116**, 68
Chabrier G., 2003, *ApJL*, **586**, L133
Chemin L., Balkowski C., Cayatte V., Carignan C., Amram P., 2006, *MNRAS*, **366**, 812
Cid Fernandes R., Gu Q., Melnick J., Terlevich E., 2004, *MNRAS*, **355**, 273
Cid Fernandes R., Mateus A., Sodré L., Stasińska G., 2005, *MNRAS*, **358**, 363
Cleveland W. S., Devlin S. J., 1988, *Journal of the American Statistical Association*, **83**, 596
Crenshaw D. M., Kraemer S. B., Gabel J. R., 2003, *AJ*, **126**, 1690
Crowl H. H., Kenney J. D. P., van Gorkom 2005, *AJ*, **130**, 65
Davis T. A., Krajnović D., McDermid R. M., Bureau M., Sarzi 2012, *MNRAS*, **426**, 1574
Dors O. L., Pérez-Montero E., Hägele G. F., 2016, *MNRAS*, **456**, 4407
Emsellem E., Greusard D., Combes F., Friedli D., Leon S., Pécontal E., Wozniak H., 2001, *A&A*, **368**, 52
Emsellem E., Goudfrooij P., Ferruit P., 2003, *MNRAS*, **345**, 1297
Englmaier P., Shlosman I., 2004, *ApJL*, **617**, L115
Erwin P., Sparke L. S., 1999, in Merritt D. R., Valluri M., Sellwood J. A., eds, *Astronomical Society of the Pacific Conference Series Vol. 182, Galaxy Dynamics - A Rutgers Symposium*. p. 243
Fathi K., van de Ven G., Peletier R. F., Emsellem E., 2005, *MNRAS*, **364**, 773
Fathi K., Storch-Bergmann T., Riffel R. A., Winge C., Axon D. J., Robinson A., Capetti A., Marconi A., 2006, *ApJL*, **641**, L25
Faúndez-Abans M., Fernandes I. F., de Oliveira-Abans M., Poppe P. C. R., Martin V. A. F., 2009, *A&A*, **507**, 1303
Faúndez-Abans M., Reshetnikov V. P., de Oliveira-Abans M., Krabbe A. C., 2015, *A&A*, **574**, A70
Ferrarese L., Freedman W. L., Hill R. J., Saha A., Madore B. F., Kennicutt Jr. R. C., Stetson 1996, *ApJ*, **464**, 568
Freeman K. C., 1970, *ApJ*, **160**, 811
Freitas-Lemes P., Rodrigues I., Faúndez-Abans M., Dors O. L., Fernandes I. F., 2012, *MNRAS*, **427**, 2772
Genzel R., Eisenhauer F., Gillessen S., 2010, *Reviews of Modern Physics*, **82**, 3121
Gordon K. D., Clayton G. C., Misselt K. A., Landolt A. U., 2003, *ApJ*, **594**, 279
Hamuy M., Walker A. R., Suntzeff N. B., Gigoux P., Heathcote S. R., Phillips M. M., 1992, *PASP*, **104**, 533
Heckman T. M., Lehnert M. D., Strickland D. K., Armus L., 2000, *ApJS*, **129**, 493
Hernquist L., 1990, *ApJ*, **356**, 359
Holmberg E., 1947, *Meddelanden fran Lunds Astronomiska Observatorium Serie II*, **120**, 1
Kenney J. D. P., van Gorkom J. H., Vollmer B., 2004, *AJ*, **127**, 3361
Knapen J. H., 2005, *Ap&SS*, **295**, 85
Knapen J. H., Shlosman I., Heller C. H., Rand. 2000, *ApJ*, **528**, 219
Kocsis B., Tremaine S., 2011, *MNRAS*, **412**, 187
Krabbe A. C., Pastoriza M. G., Winge C., Rodrigues I., 2011, *MNRAS*, **416**, 38

- Laine S., van der Marel R. P., Rossa J., Hibbard 2003, [AJ](#), **126**, 2717
- Lamareille F., Brinchmann J., Contini T., Walcher C. J., 2009, [A&A](#), **495**, 53
- Li J.-T., Wang Q. D., 2013, [MNRAS](#), **428**, 2085
- Linden T., 2014, in Sjouwerman L. O., Lang C. C., Ott J., eds, IAU Symposium Vol. 303, The Galactic Center: Feeding and Feedback in a Normal Galactic Nucleus. pp 403–413, [doi:10.1017/S1743921314001021](#)
- Lu J. R., Ghez A. M., Hornstein S. D., Morris M. R., 2009, [ApJ](#), **690**, 1463
- Maciejewski W., 2004, [MNRAS](#), **354**, 892
- Maciejewski W., Teuben P. J., Sparke L. S., 2002, [MNRAS](#), **329**, 502
- Marconi A., Axon D. J., Capetti A., Maciejewski W., Atkinson J., Batcheldor D., Binney J., 2003, [ApJ](#), **586**, 868
- Martini P., Regan M. W., Mulchaey J. S., Pogge R. W., 2003, [ApJ](#), **589**, 774
- Mateus A., Sodré L., Cid Fernandes R., Stasińska G., 2006, [MNRAS](#), **370**, 721
- Mazzalay X., Maciejewski W., Erwin P., Saglia R. P., 2014, [MNRAS](#), **438**, 2036
- McMillan P. J., 2011, [MNRAS](#), **414**, 2446
- Onodera S., Koda J., Sofue Y., Kohno K., 2004, [PASJ](#), **56**, 439
- Pasha I. I., Smirnov M. A., 1982, [Ap&SS](#), **86**, 215
- Paumard T., Genzel R., Martins F., Nayakshin S., 2006, [ApJ](#), **643**, 1011
- Phillips A. C., 1993, [AJ](#), **105**, 486
- Plummer H. C., 1911, [MNRAS](#), **71**, 460
- Pogge R. W., Martini P., 2002, [ApJ](#), **569**, 624
- Prieto M. A., Maciejewski W., Reunanen J., 2005, [AJ](#), **130**, 1472
- Repetto P., Rosado M., Gabbasov R., Fuentes-Carrera I., 2010, [AJ](#), **139**, 1600
- Riffel R. A., Storch-Bergmann T., 2011, [MNRAS](#), **411**, 469
- Riffel R. A., Storch-Bergmann T., Winge C., McGregor P. J., Beck T., Schmitt H., 2008, [MNRAS](#), **385**, 1129
- Riffel R. A., Storch-Bergmann T., Winge C., 2013, [MNRAS](#), **430**, 2249
- Rogstad D. H., 1971, [A&A](#), **13**, 108
- Rupke D. S. N., Veilleux S., 2015, [ApJ](#), **801**, 126
- Rupke D. S., Veilleux S., Sanders D. B., 2005, [ApJS](#), **160**, 87
- Schnorr-Müller A., Storch-Bergmann T., Nagar N. M., Ferrari F., 2014, [MNRAS](#), **438**, 3322
- Schödel R., Merritt D., Eckart A., 2009, [A&A](#), **502**, 91
- Sharp N. A., Keel W. C., 1985, [AJ](#), **90**, 469
- Shlosman I., Begelman M. C., Frank J., 1990, [Natur](#), **345**, 679
- Silchenko O. K., Burenkov A. N., Vlasjuk V. V., 1999, [AJ](#), **117**, 826
- Storch-Bergmann T., Dors Jr. O. L., Riffel R. A., Fathi K., 2007, [ApJ](#), **670**, 959
- Storch-Bergmann T., Lopes R. D. S., McGregor P. J., Riffel R. A., Beck T., Martini P., 2010, [MNRAS](#), **402**, 819
- Terlouw J. P., Vogelaar M. G. R., 2012, Kapteyn Package, version 2.2. Kapteyn Astronomical Institute, Groningen
- Tripe S., Gillessen S., Gerhard O. E., Bartko H., 2008, [A&A](#), **492**, 419
- Väisänen P., Ryder S., Mattila S., Kotilainen J., 2008, [ApJL](#), **689**, L37
- Vollmer B., 2009, [A&A](#), **502**, 427
- Vollmer B., Soida M., Beck R., Urbanik M., 2007, [A&A](#), **464**, L37
- Vollmer B., Soida M., Chung A., van Gorkom 2008, [A&A](#), **483**, 89
- Vollmer B., Wong O. I., Braine J., Chung A., Kenney J. D. P., 2012, [A&A](#), **543**, A33
- Wu Q., Cao X., Ho L. C., Wang D.-X., 2013, [ApJ](#), **770**, 31
- de Vaucouleurs G., 1958, [ApJ](#), **127**, 487
- de Vaucouleurs G., de Vaucouleurs A., Corwin Jr. H. G., Buta R. J., Paturel G., Fouque P., 1991, [SkyTel](#), **82**, 621